$\pi\pi$ Scattering and the Meson Resonance Spectrum

W.M. Kloet

Department of Physics and Astronomy, Rutgers University, PO Box 849, Piscataway, New Jersey 08855-0849, USA

B. Loiseau

*Division de Physique Théorique *, Institut de Physique Nucléaire, F-91406, Orsay CEDEX and LPTPE, Université P. & M. Curie, 4 Place Jussieu, 75252, Paris CEDEX 05, France*

(February 9, 2008)

Abstract

A $\pi\pi$, $\bar{K}K$, and $\rho\rho(\omega\omega)$ fully coupled channel model is used to predict the lowest isospin S, P, D, F-wave phase shifts and inelasticities for elastic $\pi\pi$ scattering from threshold to 2.0 GeV. As input the S-matrix is required to exhibit poles corresponding to the meson resonance table of the Particle Data Group. As expected, the $\pi\pi$ inelasticity is very strongly related to the opening of the $\bar{K}K$ channel near 1 GeV, and the opening of $\rho\rho(4\pi)$ and $\omega\omega(6\pi)$ channels in the 1.5 GeV region. The predictions of this model are compared to the various elastic $\pi\pi \to \pi\pi$ amplitudes, that were obtained from analyses of π^- p $\to \pi^-\pi^+$ n data. The role of the various resonances, in particular the glueball candidate $f_0(1500)$ and the $f_J(1710)$ is investigated.

PACS:13.75.Lb; 14.40.-n; 13.25.-k; 12.39.Pn

---

*Unité de Recherche des Universités Paris 11 et Paris 6 Associée au CNRS

I. INTRODUCTION

In heavy ion collisions and in anti-nucleon physics many pions are produced in the final state. Pion-pion scattering therefore plays an important role in the final state interaction of these processes. Our knowledge of $\pi\pi$ scattering is incomplete, in particular above $M_{\pi\pi} \approx$ 1 GeV. The dynamics of $\pi\pi$ scattering is often described by effective meson-exchange in the t-channel. The mechanism of t-channel exchange works very well in, for example, nucleon-nucleon scattering. However, for $\pi\pi$ scattering one may also consider the presence of the many resonances in the s-channel, a feature that is typical for $\pi\pi$ scattering but not for nucleon-nucleon scattering. A list of relevant meson resonances with their properties can be obtained from the compilation of the Particle Data Group [1]. For energies larger than 1 GeV, an additional aspect is the strong coupling of the $\pi\pi$ channel to $\bar{K}K$ and multi-pion channels, for example, four and six pions.

Previous models for S-wave $\pi\pi$ scattering have been applied from threshold to 1.4 GeV. For example, separable potential models have been considered in an approach [2–5] in which the major focus was to obtain the proper low energy behavior of the $\pi\pi$ S-wave phase shift, using the right combination of attraction and repulsion in the diagonal $\pi\pi$ interaction, and also to better understand the structure of the meson resonance $f_0(980)$. More sophisticated one-meson exchange models [6–8] have been used up to 2 GeV, still within the framework of coupling $\pi\pi$ and $\bar{K}K$ channels.

In an earlier paper [9] we reported on results within a coupled three-channel model for S-wave scattering in the 1.0 – 2.0 GeV energy region, and we were encouraged by its results when compared to the then available S-wave data. The relevant experimental $\pi\pi$ phase shifts and inelasticities, specifically $\pi^+\pi^-$, can be found from the analysis by Protopopescu et al [10], Grayer et al [11], Hyams et al [12], Bugg et al [13] and Kaminsky et al [14]. These groups have extracted the pion-pion scattering amplitudes in the $M_{\pi\pi} = 0.60$ – 1.78 GeV region by obtaining them from an analysis of the reaction π^- p $\rightarrow \pi^-\pi^+$ n. Kaminsky et al included also data from the same reaction with a polarized proton target, which allowed them to separate the contributions due to π and a_1 exchange. The low energy $\pi\pi$ data were published by Ref. [15]. From all these extracted data for the reaction $\pi^+\pi^- \rightarrow \pi^+\pi^-$ it is apparent that there is a rather strong energy dependence of the phase shifts as well as the inelasticities for S, P, D and F-wave $\pi^+\pi^-$ elastic scattering. We do not know of any data above 1.78 GeV, so a model reproducing the existing data may eventually also serve as a basis for extrapolation to higher energies. Such an extrapolation would be required to study for example the final state interaction in the process $\bar{p}p \rightarrow \pi^+\pi^-$ [16].

In view of the presence of an extensive set of resonances as given by the Particle Data Group [1], we have opted in this paper for inclusion of the various known resonances in our model for $\pi\pi$ scattering. One can then address the question, what is the role of these resonances for elastic $\pi\pi$ scattering in the various partial waves in the region of 0.3 – 2.0 GeV. In the energy range up to 2.0 GeV the dominant channels are $\pi\pi$, $\bar{K}K$, $\rho\rho$ and $\omega\omega$. Within our model, as no spin effects have been taken into account, the $\rho\rho$ and $\omega\omega$ channels can be described by a single effective channel, e.g. $\rho\rho$.

For example, the set of S-wave resonances that play a role for the $\pi\pi$ channel are the $f_0(980)$ and $f_0(1370)$ resonances, but one should also include the recently discovered $f_0(1500)$. While many conjectures about the nature of the $f_0(1500)$ have been made, its

role for $\pi\pi$ scattering is still an open question, and therefore will be one of the questions addressed in this paper. Another question is the J value of the reported $f_J(1710)$ resonance. So far one only agrees that J should be even [1]. In this approach one can study the implications of the presence of an isoscalar $f_0(1710)$ resonance for S-wave $\pi\pi$ scattering, as well as the implications of the existence of an isoscalar $f_2(1710)$ resonance for D-wave $\pi\pi$ scattering. In practice we will impose the condition that the scattering matrix, corresponding to a particular angular momentum, should have poles at the complex energies of known resonances with appropriate quantum numbers and, from this input, one can study the implications for $\pi\pi$ scattering.

The model that we will describe, can be applied for any angular momentum. In this paper it will be applied for S, P, D and F-waves. For each angular momentum the important input will be the location of the corresponding resonances as given by the Particle Data Group [1]. Sections II and III describe the model and show the analytic expressions of the S-matrix for the various angular momenta. In sections IV and V the results for respectively $l = 0$ and $l = 2$ are discussed. This order of angular momenta is chosen because the resonance $f_J(1710)$ may either contribute to the S-wave or D-wave scattering. Then the results for $l = 1$ and $l = 3$ are described in sections VI and VII respectively. Finally a discussion of all results and conclusions follows in section VIII.

II. MODEL

As in Ref. [9] we consider three coupled channels of $\pi\pi$, $\bar{K}K$ and $\rho\rho$, and label them respectively with the channel index $i = 1, 2, 3$. Our method of derivation of the scattering amplitude is generalized to all angular momenta. For each angular momentum l the Lippmann-Schwinger equation for the ij-element of the T-matrix at total invariant energy squared s, is

$$< p|T^l_{ij}(s)|q >=< p|V^l_{ij}|q > -\frac{1}{2\pi^2}\sum_{k=1}^{3}\int dp' p'^2 < p|V^l_{ik}|p' > G_k(p',s) < p'|T^l_{kj}(s)|q > . \quad (1)$$

Here $G_k(p',s)$ is the propagator for channel k and V^l_{ij} is part of the potential. In this case the potential as well as the T-matrix are both 3x3 matrices.

We choose a separable form of the potential matrix elements for each angular momentum l

$$< p|V^l_{ij}|q >= g^l_i(p)\lambda^l_{ij}g^l_j(q). \quad (2)$$

As a consequence the T-matrix elements for each l are also separable

$$< p|T^l_{ij}(s)|q >= g^l_i(p)\tau^l_{ij}(s)g^l_j(q), \quad (3)$$

where τ^l_{ij} satisfies

$$\tau^l_{ij}(s) = \lambda^l_{ij} - \sum_{k=1}^{3}\lambda^l_{ik}X^l_k(s)\tau^l_{kj}(s). \quad (4)$$

The functions X^l_k are defined in terms of the propagator G_k and vertex functions g^l_k

$$X_k^l(s) = \frac{1}{2\pi^2} \int dp' p'^2 g_k^l(p') G_k(p', s) g_k^l(p'), \tag{5}$$

and the functions $\tau_{ij}^l(s)$ can be obtained in closed form.

In the following we will suppress as much as possible the label l of the angular momentum. For example if the matrix A for a given angular momentum l is defined by

$$A_{ij} = \lambda_{ij} + \lambda_{ij} X_j, \tag{6}$$

the element τ_{11} has the general form

$$\tau_{11} = \frac{(1 + \lambda_{22} X_2)(1 + \lambda_{33} X_3) - \lambda_{23} X_3 \lambda_{32} X_2}{det(A)}. \tag{7}$$

The elastic $\pi\pi$ scattering amplitude for angular momentum l is then given by the corresponding element T_{ij} with $i = 1$ and $j = 1$, of the T-matrix of Eq. (3). The model has a resonance of angular momentum l if the corresponding T-matrix has a pole in the complex energy plane at an energy whose real part is the resonance mass and whose imaginary part is half the resonance total width. Such a pole corresponds to a zero of $det(A)$ at that complex energy, as can be seen from Eq. (7). The full expression for $det(A)$ is

$$\begin{aligned} det(A) = (1 + \lambda_{11} X_1)(1 + \lambda_{22} X_2)(1 + \lambda_{33} X_3) - \lambda_{23} X_3 \lambda_{32} X_2 (1 + \lambda_{11} X_1) \\ - \lambda_{12} X_2 \lambda_{21} X_1 (1 + \lambda_{33} X_3) - \lambda_{13} X_3 \lambda_{31} X_1 (1 + \lambda_{22} X_2) \\ + (\lambda_{13} \lambda_{32} \lambda_{21} + \lambda_{12} \lambda_{23} \lambda_{31}) X_1 X_2 X_3, \end{aligned} \tag{8}$$

with the couplings λ_{ij}^l satisfying

$$\lambda_{ji}^l = \lambda_{ij}^l. \tag{9}$$

We choose the form factor $g_i^l(p)$ of Eq. (2) to be

$$g_i^l(\beta, p) = \sqrt{\frac{4\pi}{m_i}} \frac{p^l}{(\beta^2 + p^2)^{l+1}}, \tag{10}$$

where β carries an index i as well as l. For the propagator $G_i(p', s)$ we take the form

$$G_i(p', s) = \frac{m_i}{p'^2 - p_i^2 - i\epsilon}, \tag{11}$$

where s is related to p_i by

$$s = 4(p_i^2 + m_i^2). \tag{12}$$

The functions X_i^l for $l = 0$ to 3, which are dependent on the range parameters β_i^l, become in this case

$$X_i^{l=0}(\beta, p, s) = \frac{1}{2\beta(\beta - ip)^2}, \tag{13}$$

$$X_i^{l=1}(\beta,p,s)=\frac{\beta^2-4i\beta p-p^2}{16\beta^3(\beta-ip)^4}, \tag{14}$$

$$X_i^{l=2}(\beta,p,s)=\frac{3\beta^4-18i\beta^3p-38\beta^2p^2+18i\beta p^3+3p^4}{256\beta^5(\beta-ip)^6}, \tag{15}$$

$$X_i^{l=3}(\beta,p,s)=\frac{5\beta^6-40i\beta^5p-131\beta^4p^2+208i\beta^3p^3+131\beta^2p^4-40i\beta p^5-5p^6}{2048\beta^7(\beta-ip)^8}. \tag{16}$$

Again the indices i and l of β and i of p are suppressed. The above expressions follow from evaluation of the integral in Eq. (5) for real values of p using the definitions Eq. (10) and Eq. (11). Details of the evaluation are given in part A of the Appendix. The integral in Eq. (5) is defined for $\mathrm{Re}(p)\geq 0$, and is dis-continuous over the unitarity cut for positive real p. Therefore it cannot be analytically continued for complex p with $\mathrm{Im}(p)<0$. However, the expressions of Eqs. (13), (14), (15), (16) are continuous and analytic for all complex momenta p, except for a pole on the negative imaginary axis, and can therefore be used as analytic continuation of $X_i^l(\beta,p,s)$ to complex values of p, even to the resonance region where $\mathrm{Im}(p)<0$. One also notes the familiar property of $X_i^l(\beta,p,s)$

$$X_i^l(\beta,p,s)=[X_i^l(\beta,-p^*,s^*)]^*. \tag{17}$$

As mentioned previously, the channels $i=1$, 2, 3 correspond to $\pi\pi$, $\bar{K}K$ and $\rho\rho$ respectively, and we use $m_1=0.1396$ GeV, $m_2=0.4937$ GeV and $m_3=0.7680$ GeV. Since no spin aspects are considered and the mass of the ω meson is very close to the mass of the ρ meson, the $\rho\rho$ channel can effectively be viewed as representing also the $\omega\omega$ channel for angular momenta where I = 0. We ignore the width of the ρ meson, and assume that 4π and 6π channels are dominated by $\rho\rho$ and $\omega\omega$ respectively. The relative momenta, p_i, in the i^{th} channel, are related by the kinematic condition

$$\frac{s}{4}=\frac{1}{4}M_{\pi\pi}^2=p_1^2+m_1^2=p_2^2+m_2^2=p_3^2+m_3^2. \tag{18}$$

This equation defines the invariant mass $M_{\pi\pi}$. For $l=0$ the form factor in coordinate space has the familiar form

$$g_i(r)=\frac{e^{-\beta_i r}}{r}. \tag{19}$$

The above method is equivalent to previously given expressions [9] for the S-wave elastic $\pi\pi$ scattering amplitude,

$$S_{11}=\frac{D(-p_1,p_2,p_3)}{D(p_1,p_2,p_3)}, \tag{20}$$

where S_{11} is the $\pi\pi$ S-matrix element. D is the Jost function, and $D=det(A)$, i.e.

$$\begin{aligned}D(p_1,p_2,p_3)=[&(R_1+\Lambda_1)(R_2+\Lambda_2)(R_3+\Lambda_3)-\Lambda_{12}^2(R_3+\Lambda_3)-\Lambda_{13}^2(R_2+\Lambda_2)\\&-\Lambda_{23}^2(R_1+\Lambda_1)+2\Lambda_{12}\Lambda_{13}\Lambda_{23}]/(R_1R_2R_3).\end{aligned} \tag{21}$$

The couplings Λ_i^l and Λ_{ij}^l as well as the functions R_i^l are dimensionless and their relation to λ_{ij}^l and X_i^l of Eq. (8) are given in Table I. Since the function X_i^l has the property given in Eq. (17), the Jost function satisfies

$$D(p_1, p_2, p_3) = [D(-p_1^*, -p_2^*, -p_3^*)]^*. \tag{22}$$

For each angular momentum $l = J$ we now require the S-matrix to have poles at the known J^π resonances. A summary of the considered resonances appears in Table II. For example, for $J^\pi = 0^+$ the resonances are $f_0(980)$, $f_0(1370)$ and $f_0(1500)$. For each angular momentum $l = J$ there are three range parameters β_i, and six couplings λ_{ij}. The three poles are then chosen at the complex energies, (Re$M_{\pi\pi}$, Im$M_{\pi\pi}$) corresponding respectively to the mass of the resonance and half its total decay width. Again for $J^\pi = 0^+$, these energies would be respectively (0.980, -0.0250), (1.300, -0.200) and (1.503, -0.060) GeV. We require $det(A)$ of Eq. (8) to have zeros at these complex energies, which leads to six constraints on the nine parameters. There are several parameter sets that satisfy the above constraints, as will be discussed below.

III. ADDITIONAL FORMALISM FOR $J^\pi = 0^+$, $I = 0$

The case $J^\pi = 0^+$ needs special attention. We have before published results [9] for a three coupled channel model as described in Section II. One obtains impressive results for phase shifts as well as inelasticities in the energy region 0.9 – 2.0 GeV. However, within the model described in Section II it is not possible to obtain a realistic description at energies below 0.9 GeV. The reason is that the potential for the $\pi\pi$ channel for the S-channel requires an attractive term as well as a repulsive one. It has been earlier demonstrated [3] that addition of a second term in the S-wave $\pi\pi$ potential is successful in describing the low energy behavior of the $l = 0$ scattering. We develop therefore a formalism, described in Appendix B, adding such an attractive term. In this paper this formalism is only applied for $l = 0$ scattering.

IV. RESULTS FOR $J^\pi = 0^+$, $I = 0$

Since our previous publication of $l = 0$ results [9], the Particle Data Group [1] has significantly revised its compilation of $J^\pi(I) = 0^+(0)$ resonances. At present it contains the resonances $f_0(980)$, $f_0(1370)$, $f_0(1500)$ and possibly $f_0(1710)$. They occur respectively at the complex energies (0.980, -0.025), (1.300, -0.200), (1.503,-0.060) and (1.697, -0.088) GeV. However, the real as well as the imaginary part of the pole positions have uncertainties and those are rather large for the $f_0(1370)$ resonance.

We are particularly interested in the role played by the "new" resonance $f_0(1500)$, which has been considered as a glueball candidate. Therefore we start by taking the first three resonances, $f_0(980)$, $f_0(1370)$ and $f_0(1500)$, as input for our model and study the consequences for the resulting $\pi\pi$ scattering parameters. These three $J = 0$ resonances together will impose constraints on the analytic expression for the S-matrix for $l = 0$. The S-matrix must have three poles at the corresponding three complex energies. These constraints determine or restrict the possible values of the model parameters $\beta_0, \beta_1, \beta_2, \beta_3, \Lambda_0, \Lambda_1, \Lambda_2, \Lambda_3, \Lambda_{12}, \Lambda_{13}$

and Λ_{23}, where, as stated in Appendix B, the index 0 labels the second potential term of the $\pi\pi$ channel. Using these parameter values, one can then immediately determine the S-submatrix S_{11}, describing $\pi\pi \to \pi\pi$ scattering. Since S_{11} for angular momentum l is parametrized by a phase shift δ and an inelasticity η, viz.

$$S_{11} = \eta e^{2i\delta}, \tag{23}$$

one obtains the values of δ and η as a function of energy. The $l = 0$ scattering parameters are then compared to experimental data.

There is still an additional freedom in our model. This is related to the location of the resonance in the complex energy plane and to the analytic structure of the S-matrix for the three coupled channels $\pi\pi$, $\bar{K}K$ and $\rho\rho$. Since the relation between energy and momentum is quadratic, for each complex resonance energy there are two corresponding complex momenta p_i for each channel, one with Im $p_i < 0$ and a second with Im $p_i > 0$. This defines two possible sheets in the complex energy plane for each channel. Because there are three channels, there are all together eight sheets. The exact location off all resonance poles with respect to these eight sheets determines the specific solution for the S-matrix.

In our standard choice of complex channel momenta p_i for each resonance, the sign of Im p_i is such that the momenta p_i are all close to the physical scattering region. The physical scattering region has positive real momenta p_i for the open channels, and positive imaginary momenta p_i for the closed channels. This means that a standard resonance corresponds to a channel momentum p_i with Im $p_i < 0$ if channel i is open and Im $p_i > 0$ if channel i is closed. The $\pi\pi$ channel is always open, the $\bar{K}K$ channel opens at $2m_K$ and the $\rho\rho$ channel opens at 2 m_ρ.

If we put all three resonances $f_0(980)$, $f_0(1370)$ and $f_0(1500)$, on the standard $\pi\pi$, $\bar{K}K$ and $\rho\rho$ sheets, i.e. near the physical region, (where all three channel momenta p_1, p_2, p_3 have the required imaginary part, in agreement with each channel being open or closed), a solution is found for the parameter set $(\beta_i, \Lambda_i, \Lambda_{ij})$ that is given in the first line of Table. III. However, the corresponding prediction for the $\pi\pi$ phase shifts is considerably lower than the data suggests, as can be seen by the dashed curve in Fig. 1. Therefore we next consider cases where one of the resonances is not close to the physical scattering region.

From the decay properties of the first three $J = 0$ resonances one knows that $f_0(980)$ and $f_0(1370)$ both have significant couplings to the $\pi\pi$ and $\bar{K}K$ channels. On the other hand the $f_0(1500)$ resonance has a preference to decay into $\eta\eta'$, $\eta\eta$, $4\pi^o$, $2\pi^o$ and $2\pi^+2\pi^-$. It is significant that the decay of $f_0(1500)$ into $\pi^+\pi^-$ and $\bar{K}K$ may be rather small. It suggests that the $f_0(1500)$ resonance could be located on the $\pi^+\pi^-$ or $\bar{K}K$ non-standard sheets (i.e. its pole location may correspond to a channel momentum p_i with a positive imaginary part).

If we choose to put $f_0(1500)$ on the non-standard $\pi^+\pi^-$ sheet, (i.e. treat it as a virtual resonance, where the relative $\pi\pi$ momentum has a positive imaginary part), there is a significant improvement of the model prediction when compared to the experimental data. The predictions for the $\pi\pi$ phase shifts and inelasticities are shown as the solid curve in Fig. 1 and Fig. 2. The corresponding parameter set is given in the second line of Table III. The behavior of phase shift and inelasticity above 1.6 GeV will be influenced further by higher resonances. On the other hand, if we put the $f_0(1500)$ resonance on the sheet, where also the relative $\bar{K}K$ momentum has a positive imaginary part, the $\pi\pi$ phase shift obtains a significant structure in the 1.2 – 1.4 GeV region. Such a structure is not present in the

experimental data. We therefore conclude that the data for $\pi^+\pi^-$ scattering are consistent with a $f_0(1500)$ resonance that is very different from the $f_0(980)$ and $f_0(1370)$ and that it couples only weakly to $\pi^+\pi^-$. At the same time these data do not require its coupling to $\bar{K}K$ to be also weak.

The next question is if these data are consistent with the existence of a $f_0(1710)$ resonance. Indeed it is possible with resonance poles at the complex masses (1.200, -0.250) and (1.697, -0.300) to obtain an excellent prediction for the phase shift in the 1.0 – 1.5 GeV region that is in good agreement with the experimental data. In Fig. 3 and Fig. 4 the S-wave phase shifts and S-wave inelasticities for three parameter sets, are shown when $f_0(1710)$ is included. In this case one requires a large width for $f_0(1710)$ as well as a low mass for the $f_0(1370)$. The corresponding three sets of parameters are given in the third to fifth line of Table III. The phase shifts in this case (see Fig. 3) show an energy dependence that is closer to the data than the model prediction in Fig. 1. This makes a strong case in favor of $J = 0$ for $f_J(1710)$. The possibility of the existence of $f_2(1710)$ still remains to be considered and the results for $J = 2$ will be discussed in the next section.

V. RESULTS FOR $J^\pi = 2^+$, $I = 0$

The Particle Data Group lists several $J^\pi(I) = 2^+(0)$ resonances, $f_2(1270)$, $f_2(1525)$ and $f_2(2010)$ with the possibility of an additional $f_2(1710)$. The first three resonances occur at complex energies (1.275, -0.092), (1.525, -0.038) and (2.011, -0.101) GeV. However, a resonance with even J has also been observed at (1.697, -0.088) GeV and we will therefore follow two avenues. First, in case A we impose on our model the existence of three resonances in $J = 2$ at complex energies (1.275, -0.092), (1.525, -0.038) and (1.607, -0.088) GeV, while in the second case B the existence of three resonances at (1.275, -0.092), (1.525, -0.038) and (2.011. -0.101) GeV will be used as a model constraint. We will subsequently discuss both cases.

In both cases we use the formulae given in Section II. The S-submatrix S_{11} for D-waves is then described by the nine parameters $\beta_1, \beta_2, \beta_3, \Lambda_1, \Lambda_2, \Lambda_3, \Lambda_{12}, \Lambda_{13}$ and Λ_{23}. The requirement that the S-matrix must have poles at the complex energies corresponding to three resonances, leads to six constraints. However, it turns out that neither case A nor case B allows a solution within our model if we demand that all three resonances are on the standard sheet for $\pi\pi$, $\bar{K}K$ and $\rho\rho$ (i.e. where all relative channel momenta have imaginary parts close to the physical region). On the other hand solutions for both cases are found, if we locate the second resonance $f_2(1525)$ on the $\pi\pi$ sheet, where the relative $\pi\pi$ momentum has a positive imaginary part. A physical interpretation of this would be that the coupling of the $f_2(1525)$ resonance to the $\pi\pi$ channel is weak, meaning that $f_2(1525)$ has a rather small decay width into $\pi\pi$. The Particle Data Group gives that $f_2(1525)$ decays for only 0.8% into $\pi\pi$ while for 88.8% into $\bar{K}K$, which would justify to put the $f_2(1525)$ pole not on the standard $\pi\pi$ sheet near the physical region, but place it on the alternative $\pi\pi$ sheet, where Im $p_{\pi\pi} > 0$. Proceeding, the model gives results for case A as well as for case B closest to the data if the third resonance is put on the non-standard $\rho\rho$ sheet.

Then for case A, which contains the $f_2(1710)$ resonance, the parameter set is given in the first line of Table IV, and the model predictions for the phase shift and inelasticity are given by the dashed line in Fig. 5 and Fig. 6 respectively. For case A a structure near 1.6

GeV is present in the phase shift, and the inelasticity is much too low in comparison to the data. There is no evidence for a similar structure in the experimental phase shift.

On the other hand, if we consider case B where there is no resonance at 1.7 GeV, but instead a resonance near 2.0 GeV, the parameter set is given on the second line of Table IV, and the corresponding model prediction for phase shift and inelasticity is represented by the solid curves in Fig. 5 and Fig. 6. In the phase shift of case B the structure near 1.6 GeV has practically disappeared, and the prediction for the phase shift (see Fig. 5) is in closer agreement with the data. At the same time one finds that for case B the predicted inelasticity (see Fig. 6) is in much better agreement with the experimental inelasticity.

It is tempting to conclude that the presence of a $f_2(1710)$ resonance would cause more structure in the $l = 2$ phase shift than has been observed experimentally, and a value of $J = 2$ for $f_J(1710)$ is therefore unlikely.

VI. RESULTS FOR $J^\pi = 1^-$, $I = 1$

Following again the formalism of Section II, the resonances imposed for $l = 1$ are $\rho(770)$, $\rho(1450)$ and $\rho(1700)$. They occur, according to the most recent compilation of the Particle Data Group, at the complex energies (0.768, -0.075), (1.465, -0.,155) (1.700, -0.118) [1] in units of GeV. Therefore the existence of these three $J = 1$ resonances again imposes the constraints that the analytic expression for the S-matrix for $l = 1$ has three poles at these three complex energies. These constraints determine the possible values of the nine model parameters, and lead to corresponding P-wave phase shifts and inelasticities. The parameter values for our model are given in the first line of Table V. The resulting phase shifts and inelasticities are shown respectively in Fig. 7 and Fig. 8 by the dashed curve. The different sets of experimental data for the $l = 1$ phase shift are in quite good agreement with each other. One observes that the model phase shifts are in good agreement with the data only below 1.3 GeV, but are too high above 1.3 GeV. The model phase shift also shows a structure near 1.6 GeV that is not present in the data. For the $l = 1$ inelasticity there is no agreement between the different experimental data sets. In one experimental set of data there is considerable inelasticity when the $\bar{K}K$ channel opens at 1 GeV, while in others the inelasticity is mainly driven by the opening of the $\rho\rho$ channel near 1.4 – 1.5 GeV. Hence it is not possible to draw any conclusions about the model predictions from the inelasticity. The model result as seen in the dashed curve in Fig. 8 has only a contribution to the inelasticity beyond the 1.4 GeV region. It is somewhat of a surprise that a treatment of $\rho(770)$, $\rho(1450)$ and $\rho(1700)$ as being very similar type resonances in all three channels, causes the model to fail for energies above 1.3 GeV.

We have explored several of the options of placing one of the resonances on another sheet. The best agreement with the experimental data is obtained if we locate the third resonance, $\rho(1700)$, on the non-standard $\bar{K}K$ sheet (i.e. Im $p_{\bar{K}K} > 0$). For this case the corresponding parameter set is given in the second line of Table V, and the corresponding prediction of the phase shift and inelasticity is given as the solid curves in Fig. 7 and Fig. 8. Comparing with the dashed curve, a dramatic improvement has been obtained for the phase shift. A structure near 1.6 – 1.7 GeV remains however present in the model. There may be an indication of some structure in one set of experimental phase shifts, but it is far from compelling. The corresponding model prediction for the inelasticity includes for this case a larger effect of

the $\bar{K}K$ channel, as shown by the solid curve in Fig. 8. As long as the experimental data for the inelasticity suffer from the considerable internal disagreement as shown in Fig. 8, it is hard to draw conclusive information from a comparison of this observable at this time. Other choices of possible sheets do not lead to further improvement of the predictions.

VII. RESULTS FOR $J^\pi = 3^-$, $I = 1$

For $J^\pi = 3^-$ there is one well established resonance $\rho_3(1690)$, at (1.691, -0.080) GeV, and a brief mentioning of $\rho_3(2250)$. Since we are interested in the phase shift below 2.0 GeV, the precise location of higher poles seems not very important. Within our model, having the essential ingredient of three channels and therefore nine parameters, a single resonance would allow too much freedom in the parameters. Just for convenience we impose therefore the condition that there are three resonances, even for $J^\pi = 3^-$, at energies (1.691, -0.080), (2.250, -0.125), (2.700, -0.300) GeV. In that case it is straightforward to obtain a good fit to the experimental phase shift and inelasticity by the parameter set given in Table VI. The model prediction for that set is given as the solid curves in Fig. 9 and Fig. 10.

VIII. DISCUSSION AND CONCLUSION

In conclusion, we have constructed a three-channel model which gives a reasonable description of the S, P, D and F-wave $\pi\pi$ scattering in the 0.3 – 1.7 GeV region. Apart from the $\pi\pi$ and $\bar{K}K$ channels, the multi-pion channels are described as effective $\rho\rho$ and $\omega\omega$ channels. As a result the model exhibits branch cuts at the $\bar{K}K$ and $\rho\rho(\omega\omega)$ thresholds. Subsequently we require the S-matrix to have poles at the three lowest known resonances for each angular momentum $J^\pi(I)$ as listed by the Particle Data Group [1]. The position of the resonances on the various complex momentum sheets reflects the decay properties of each resonance.

As a by-product of this investigation one concludes that the $f_0(1500)$ resonance plays a role in S-wave $\pi^+\pi^-$ scattering that is quite different from that of $f_0(980)$ and $f_0(1370)$. Also the S-wave and D-wave $\pi^+\pi^-$ scattering data seem to be in better agreement with a value of $J = 0$ for $f_J(1710)$ and at the same time in disagreement with a value of $J = 2$. A further surprise for the $J^\pi(I) = 1^-(1)$ meson resonances is that not all three resonances $\rho(770)$, $\rho(1450)$, $\rho(1700)$, play a similar role in all three channels of this model.

In order to establish how model dependent these conclusions are, it would be interesting to study the role of the various resonances off all angular momenta in other approaches [5,7]. The present model can also be extremely useful to describe the final state interaction in reactions like $\bar{p}p \to \pi^+\pi^-$ [16].

ACKNOWLEDGMENTS

One of the authors (W.M.K.) is grateful to the Division de Physique Théorique, Institut de Physique Nucléaire at Orsay for its hospitality during his stay, when this work was

initiated. Both authors thank W.R. Gibbs, L. Leśniak, J. de Swart and R. Vinh Mau for helpful discussions. This work is supported in part by NSF Grant No. PHYS-9504866.

APPENDIX A: Integrals for $X^l(s)$

In order to evaluate the integrals for $X^l(p,s)$ of Eq. (5), using Eq. (10) and (11), i.e.

$$X^l(p,s) = \frac{2}{\pi}\int dp' p'^2 \frac{p'^{2l}}{(p'^2+\beta^2)^{2l+2}} \frac{1}{p'^2 - p^2 - i\epsilon}, \tag{24}$$

for real p, we define a function $Z^l(p,s)$ by

$$Z^l(p,s) = \frac{2}{\pi}\int dp' p'^2 \frac{1}{(p'^2+\beta^2)^{l}} \frac{1}{p'^2 - p^2 - i\epsilon}, \tag{25}$$

also for real values of p. The values of $Z^l(p,s)$ for $l > 1$ can be determined, using the iteration method of the Appendix of Ref. [17],

$$Z^{l+1}(p,s) = -\frac{1}{l}\frac{\partial}{\partial\beta^2} Z^l(p,s). \tag{26}$$

All expressions for $Z^{l+1}(p,s)$ can then be determined from

$$Z^1(p,s) = \frac{1}{\beta - ip}. \tag{27}$$

The expression of Eq. (27) for real p can again be analytically continued for complex p.

The expressions for $X^l(p,s)$ follow from the binomial forms

$$X^0(p,s) = Z^2(p,s), \tag{28}$$

$$X^1(p,s) = Z^3(p,s) - \beta^2 Z^4(p,s), \tag{29}$$

$$X^2(p,s) = Z^4(p,s) - 2\beta^2 Z^5(p,s) + \beta^4 Z^6(p,s), \tag{30}$$

$$X^3(p,s) = Z^5(p,s) - 3\beta^2 Z^5(p,s) + 3\beta^4 Z^7(p,s) - \beta^6 Z^8(p,s). \tag{31}$$

APPENDIX B: Formulae with a second term in the $\pi\pi$ potential for the $l = 0$ scattering.

We give here explicit formulae for the Jost function and for the scattering length when we add, as in Ref. [2], a second term in the $\pi\pi$ channel for the $l = 0$ scattering. The potential as well as the T-matrix of Eq. (1) are then 4x4 matrices. We choose the index 0 to label this new term in the $\pi\pi$ potential of range β_0 and strength λ_{00}. We do not introduce

any coupling between this term and the $\bar{K}K$ and $\rho\rho$ channels, i.e. $\lambda_{0i} = 0$ for $i = 2, 3$ and furthermore $\lambda_{01} \equiv 0$.

The new Jost function can then be obtained in a similar way to the derivation performed in section II. One gets

$$D(p_1p_2, p_3) = \left(1 + \frac{\Lambda_0}{R_0}\right) Q(p_2, p_3) + \left[1 + \frac{\Lambda_0}{R_0}\left(\frac{\beta_1 - \beta_0}{\beta_1 + \beta_0}\right)^2\right] \frac{P(p_2, p_3)}{R_1}. \tag{32}$$

Here $\Lambda_0 = \lambda_{00}/(2\beta_0^3)$ and $R_0 = 1/(2\beta_0^3 X_0)$ with, as in Eq. (13),

$$X_0 = \frac{1}{2\beta_0(\beta_0 - ip_1)^2}. \tag{33}$$

Eq. (32) contains the expressions

$$Q(p_2, p_3) = 1 + \frac{\Lambda_2}{R_2} + \frac{\Lambda_3}{R_3} + \frac{\Lambda_2\Lambda_3 - \Lambda_{23}^2}{R_2R_3}, \tag{34}$$

$$P(p_2, p_3) = 1 + \frac{\Lambda_1\Lambda_2 - \Lambda_{12}^2}{R_2} + \frac{\Lambda_1\Lambda_3 - \Lambda_{13}^2}{R_3} + \frac{L_{123}}{R_2R_3}, \tag{35}$$

with

$$L_{123} = 2\Lambda_{12}\Lambda_{23}\Lambda_{13} - \Lambda_{13}^2\Lambda_2 - \Lambda_{12}^2\Lambda_3 - \Lambda_{23}^2\Lambda_1 + \Lambda_1\Lambda_2\Lambda_3. \tag{36}$$

It can be seen that if $\Lambda_0 = 0$, Eq. (32) reduces to Eq. (21) as it should.

The $\pi\pi$ scattering length can be calculated as

$$a_{\pi\pi} = \lim_{p_1 \to 0} \frac{S_{11} - 1}{2ip_1} = \lim_{p_1 \to 0} \frac{D(-p_1, p_2, p_3) - D(p_1, p_2, p_3)}{2ip_1 D(p_1, p_2, p_3)}. \tag{37}$$

As $\lim_{p_1 \to 0} A_1 = 1$, one obtains

$$a_{\pi\pi} = \frac{-2P(p_2, p_3)/\beta_1 - 2\Lambda_0/\beta_0 \left[Q(p_2, p_3) + P(p_2, p_3)\frac{(\beta_1 - \beta_0)^2}{\beta_1(\beta_1 + \beta_0)}\right]}{Q(p_2, p_3)(1 + \Lambda_0) + P(p_2, p_3)\left[1 + \Lambda_0\left(\frac{\beta_1 - \beta_0}{\beta_1 + \beta_0}\right)^2\right]}. \tag{38}$$

In Eq. (38) $p_2^2 = m_1^2 - m_2^2$ and $p_3^2 = m_1^2 - m_3^2$.

REFERENCES

[1] R.M. Barnett et al (Particle Data Group), Phys.Rev. D **54**, 1 (1996).
[2] F. Cannata, J.P. Dedonder, L. Leśniak, Phys.Lett. B **207**, 115 (1988).
[3] F. Cannata, J.P. Dedonder, L. Leśniak, Z. Phys. A **334**, 457 (1989).
[4] F. Cannata, J.P. Dedonder, L. Leśniak, Z. Phys. A **343**, 451 (1992).
[5] R. Kamiński, L. Leśniak and J.-P. Maillet, Phys.Rev. D **50**, 3145 (1994).
[6] D. Lohse, J.W. Durso, K. Holinde, J. Speth, Phys. Lett. B **234**, 235 (1990); Nucl.Phys. A **516**, 511 (1990).
[7] V. Mull, K. Holinde, J. Speth, Phys.Lett. B **275**, 12 (1992).
[8] B.C. Pearce, private communication.
[9] W.M. Kloet and B. Loiseau, Z. Phys. A **353**, 227 (1995).
[10] S. Protopopescu et al, Phys. Rev. D **7**, 1279 (1973).
[11] G. Grayer et al, Nucl.Phys. B **75**, 189 (1974).
[12] B. Hyams et al , Nucl. Phys. B **100**, 205 (1975).
[13] D.V. Bugg, A.V. Sarantsev, B.S. Zou, Nucl. Phys. B **471**, 59 (1996).
[14] R. Kamiński, L. Leśniak and K. Rybicki, Acta Phys Pol B **27**, 3259 (1996).
[15] L. Rosselet et al, Phys.Rev. D **15**, 574 (1977).
[16] G. Bathas and W.M. Kloet, Phys. Rev. C **47**, 2207 (1993).
[17] W. Gibbs, B. Loiseau, Phys.Rev. C **50**, 2742 (1994).

FIGURES

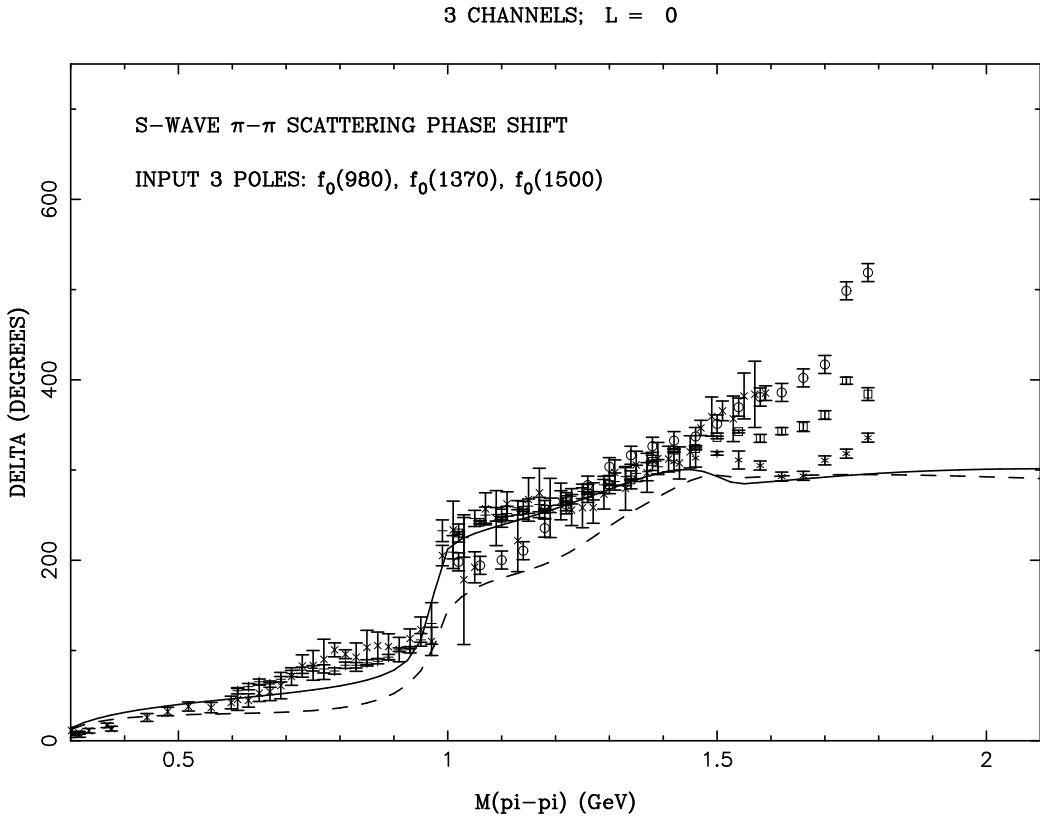

FIG. 1. S-wave $\pi\pi$ phase shifts from the three-channel model, if poles are present for $f_0(980)$, $f_0(1370)$ and $f_0(1500)$. The dashed curve is the result for $l = 0$ if the $f_0(1500)$ pole occurs at Im $p_{\pi\pi} < 0$ with the parameter set of the first line in Table III. The solid curve is the prediction for the parameter set in the second line in Table III, where the $f_0(1500)$ resonance pole corresponds to Im $p_{\pi\pi} > 0$. Data are from Refs. [11,12,14].

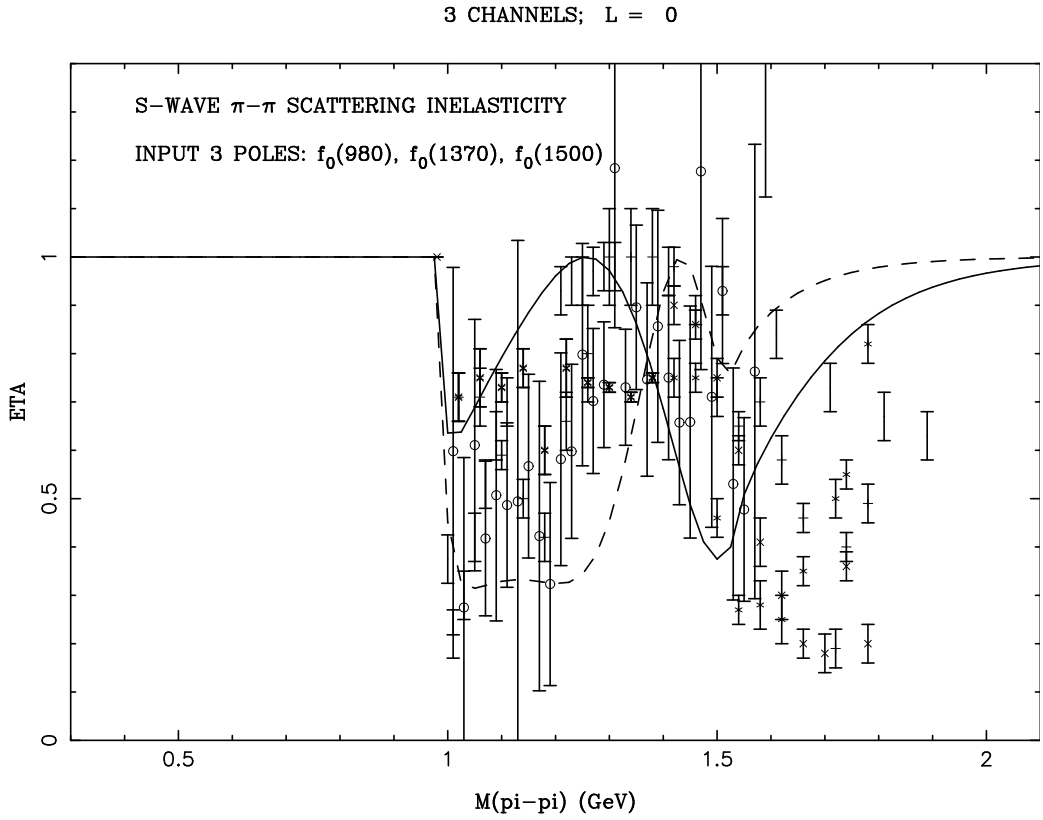

FIG. 2. S-wave $\pi\pi$ inelasticities from the three-channel model, if poles are present for $f_0(980)$, $f_0(1370)$ and $f_0(1500)$. The dashed curve is the result for $l = 0$ if $f_0(1500)$ has Im $p_{\pi\pi} < 0$ and the parameters of the first line in Table III. Solid curve is the prediction for the parameter set in the second line in Table III, where $f_0(1500)$ has Im $p_{\pi\pi} > 0$. Data are from Refs. [11,12,14].

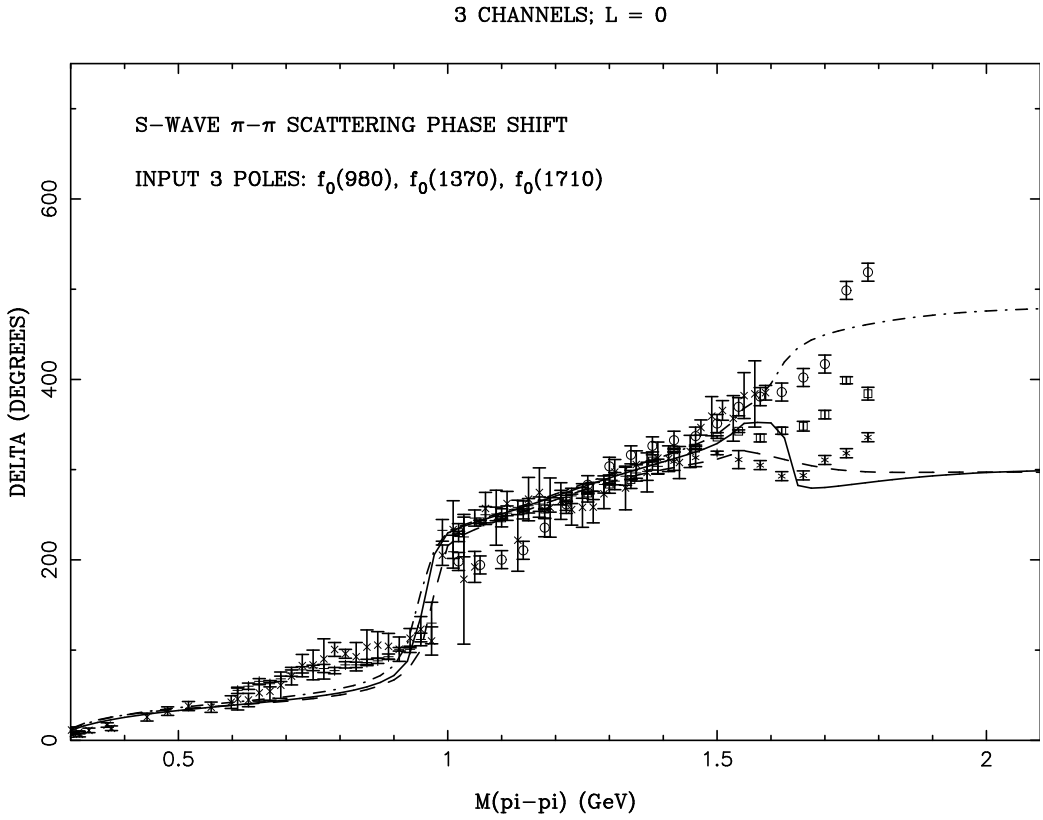

FIG. 3. S-wave $\pi\pi$ phase shifts from the three-channel model, if poles are present for $f_0(980)$, $f_0(1370)$ and $f_0(1710)$. Solid, dashed and dash-dotted curves are the prediction for $l = 0$ parameter sets from Table III, lines three thru five. Data are as in Fig. 1.

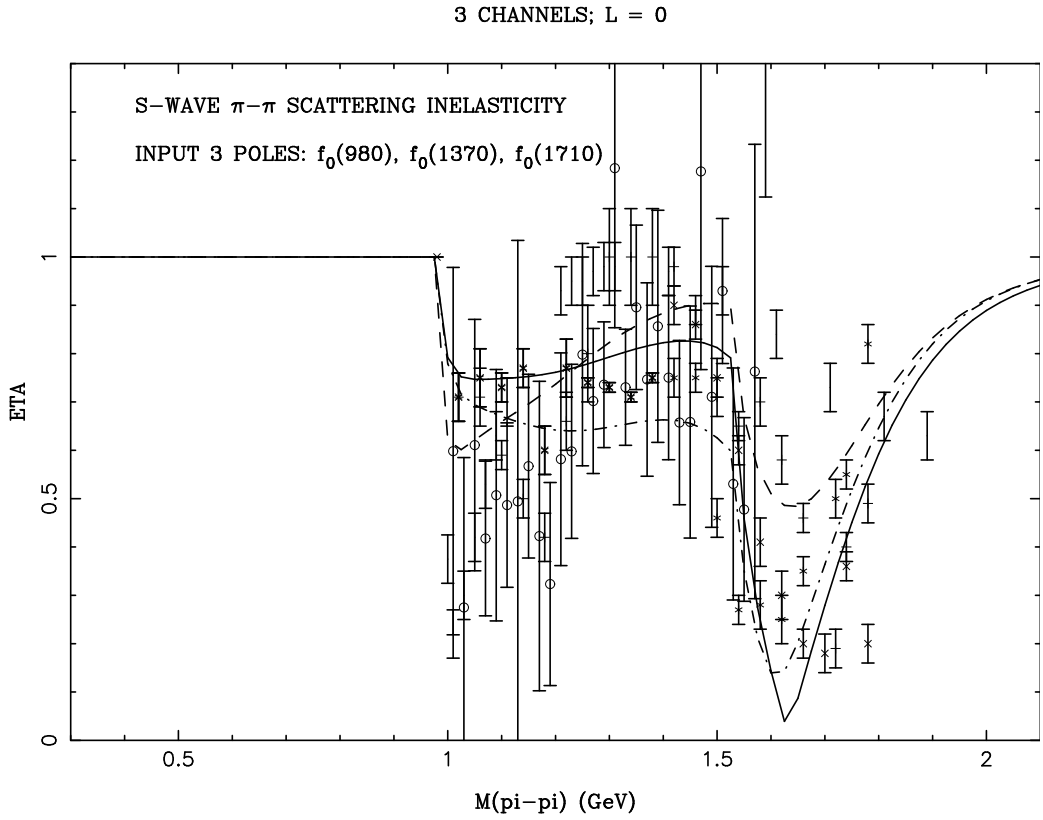

FIG. 4. S-wave $\pi\pi$ inelasticities from the three-channel model, if poles are present for $f_0(980)$, $f_0(1370)$ and $f_0(1710)$. Curves are as in Fig. 3. Data are as in Fig. 2.

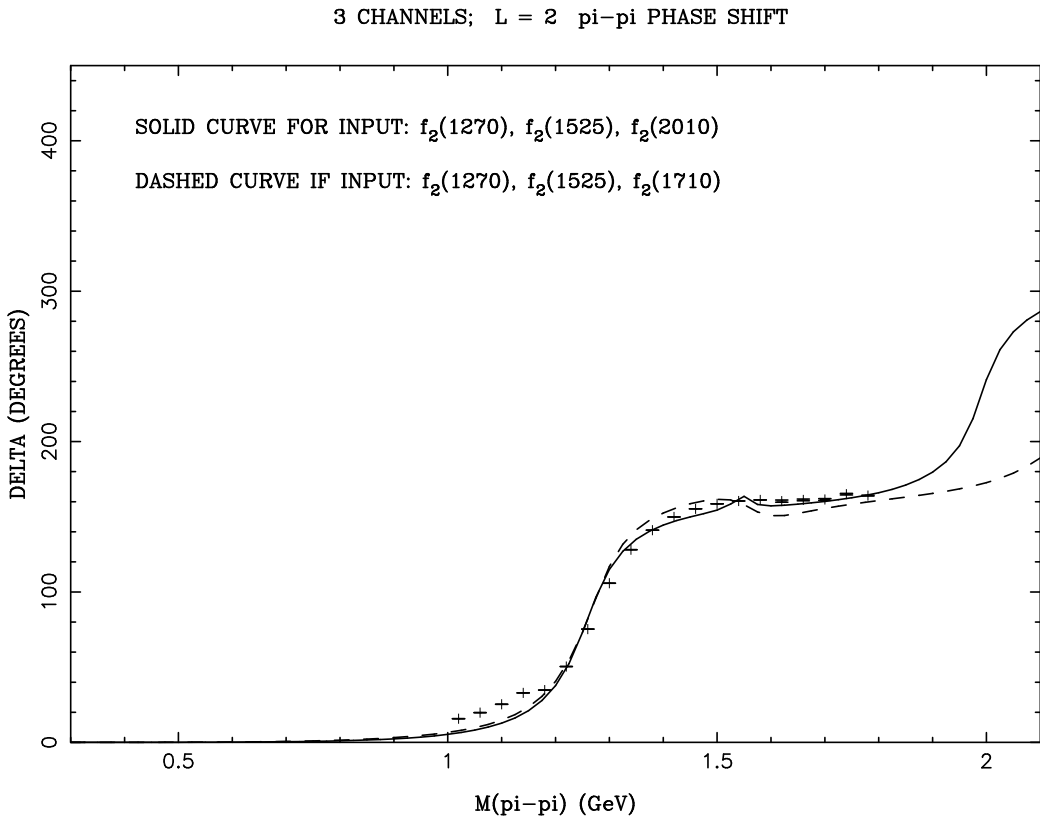

FIG. 5. D-wave $\pi\pi$ phase shifts from the three-channel model, if poles are present for $f_2(1270)$, $f_2(1525)$ and $f_2(2010)$. Dashed curve is the prediction from the first $l = 2$ parameter set from Table IV, case A, with the $f_2(1525)$ resonance with Im $p_{\pi\pi} > 0$, while the third resonance is the $f_2(1710)$. Solid curve is the prediction from the second $l = 2$ parameter set from Table IV, case B, with the $f_2(1525)$ resonance with Im $p_{\pi\pi} > 0$, while the third resonance is the $f_2(2010)$. Data are from Ref. [12].

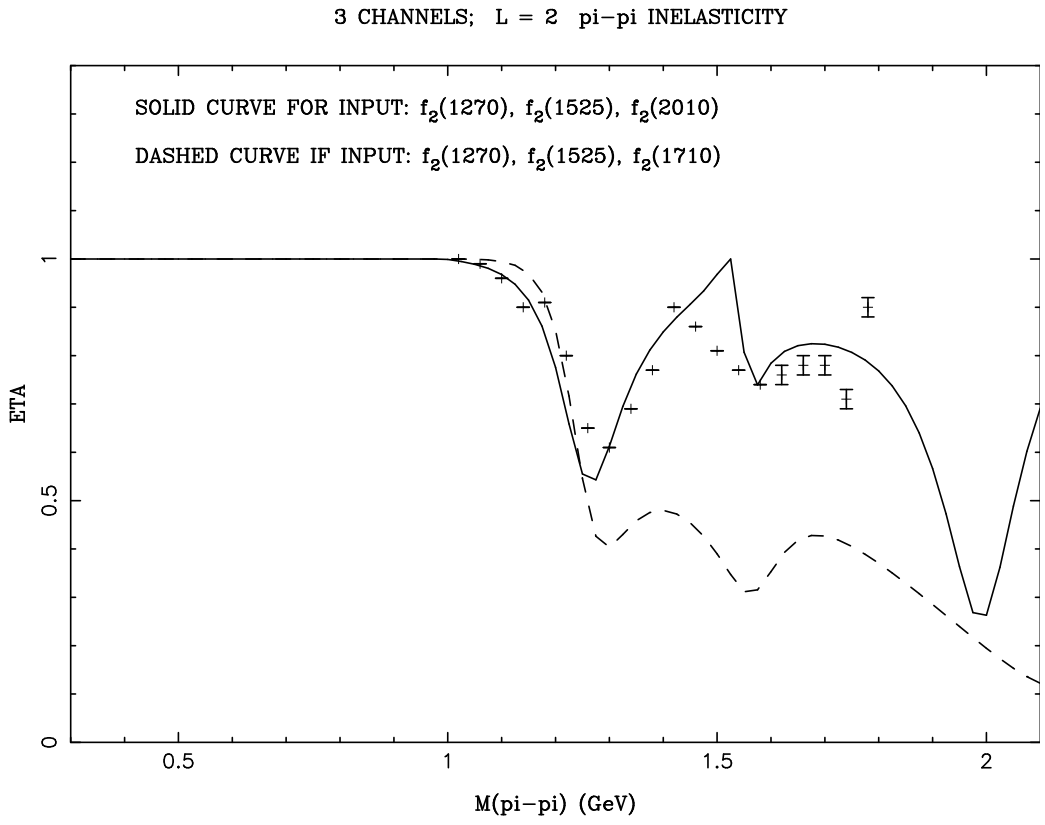

FIG. 6. D-wave $\pi\pi$ inelasticities from the three-channel model, if poles are present for $f_2(1270)$, $f_2(1525)$ and $f_2(2010)$. Dashed and solid curves are as in Fig. 5. Data are from Ref. [12].

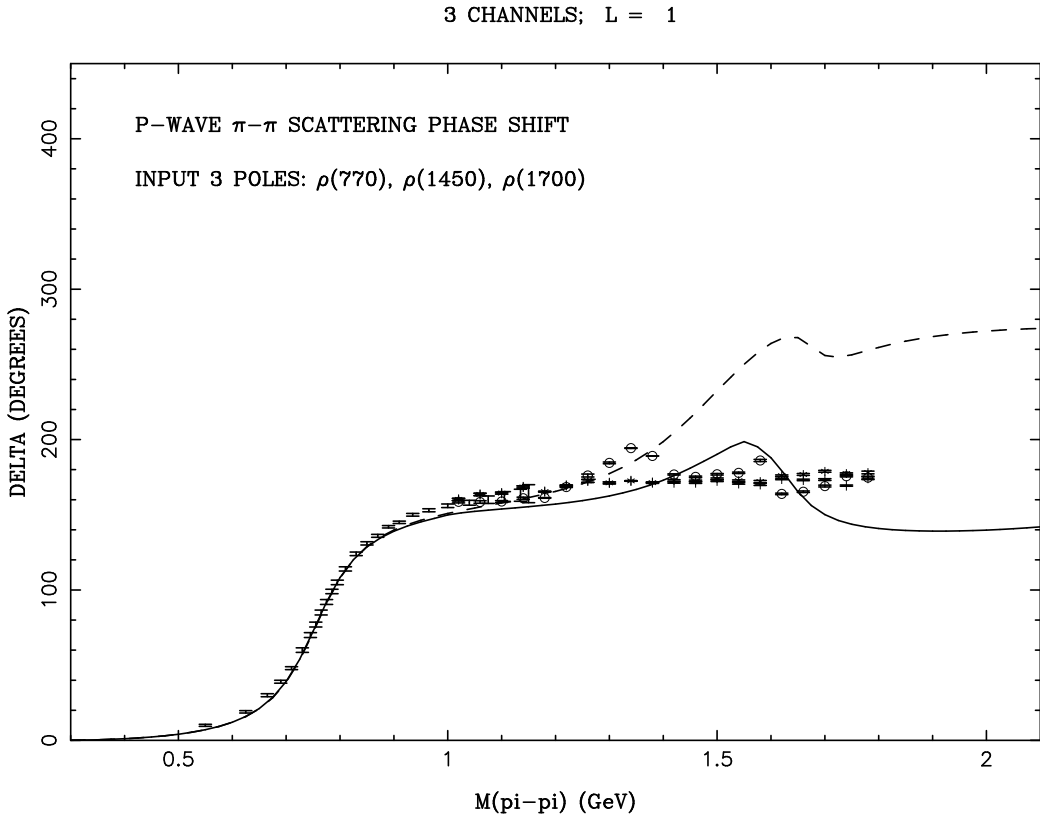

FIG. 7. P-wave $\pi\pi$ phase shifts (in degrees) from various experimental analyses. The curves represent $\pi\pi$ phase shifts for $l = 1$ from the three-channel model, if poles are present for $\rho(770)$, $\rho(1450)$ and $\rho(1700)$. The dashed curve has all resonances on the standard $\pi\pi$, $\bar{K}K$ and $\rho\rho$ sheets, while the solid curve is the result if $\rho(1700)$ is located on the sheet where Im $p_{\bar{K}K} > 0$. Data points are from Refs. [10,12].

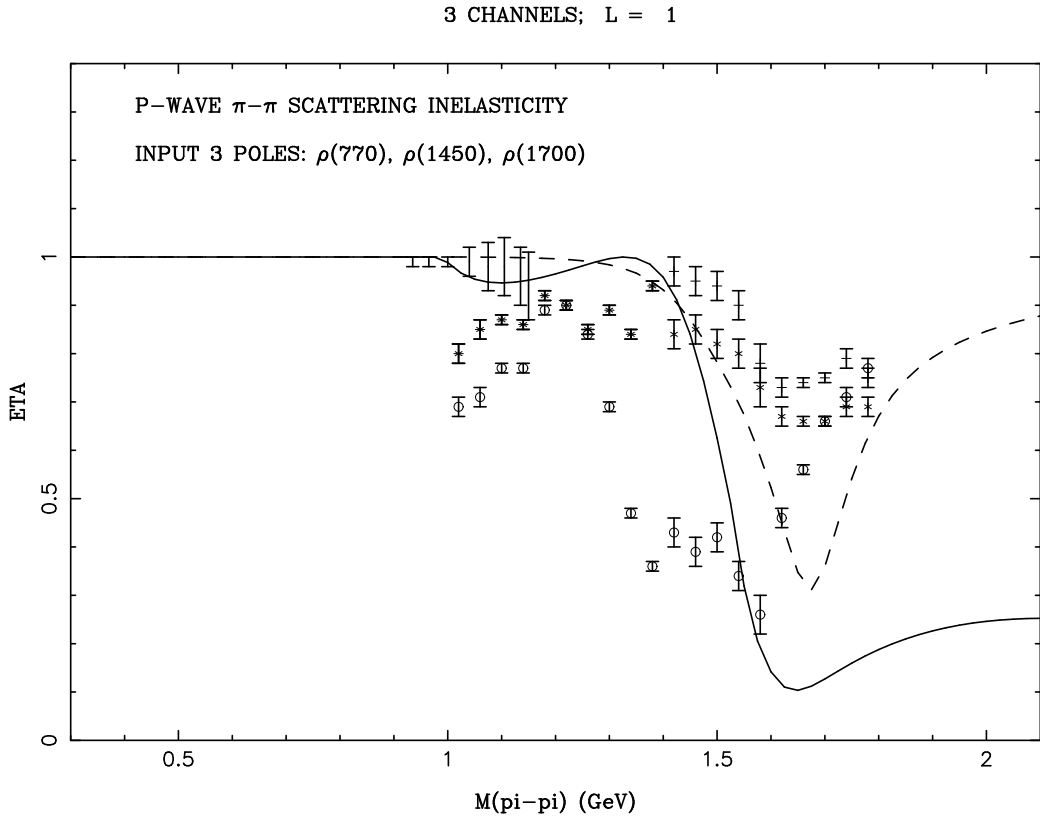

FIG. 8. P-wave $\pi\pi$ inelasticities from various experimental analyses. The curves represent $\pi\pi$ inelasticities for $l = 1$ from the three-channel model, if poles are present for $\rho(770)$, $\rho(1450)$ and $\rho(1700)$. The dashed curve has all resonances on the standard $\pi\pi$, $\bar{K}K$ and $\rho\rho$ sheets, while the solid curve is the result if $\rho(1700)$ is located on the sheet where Im $p_{\bar{K}K} > 0$. Data points are from Ref. [10,12].

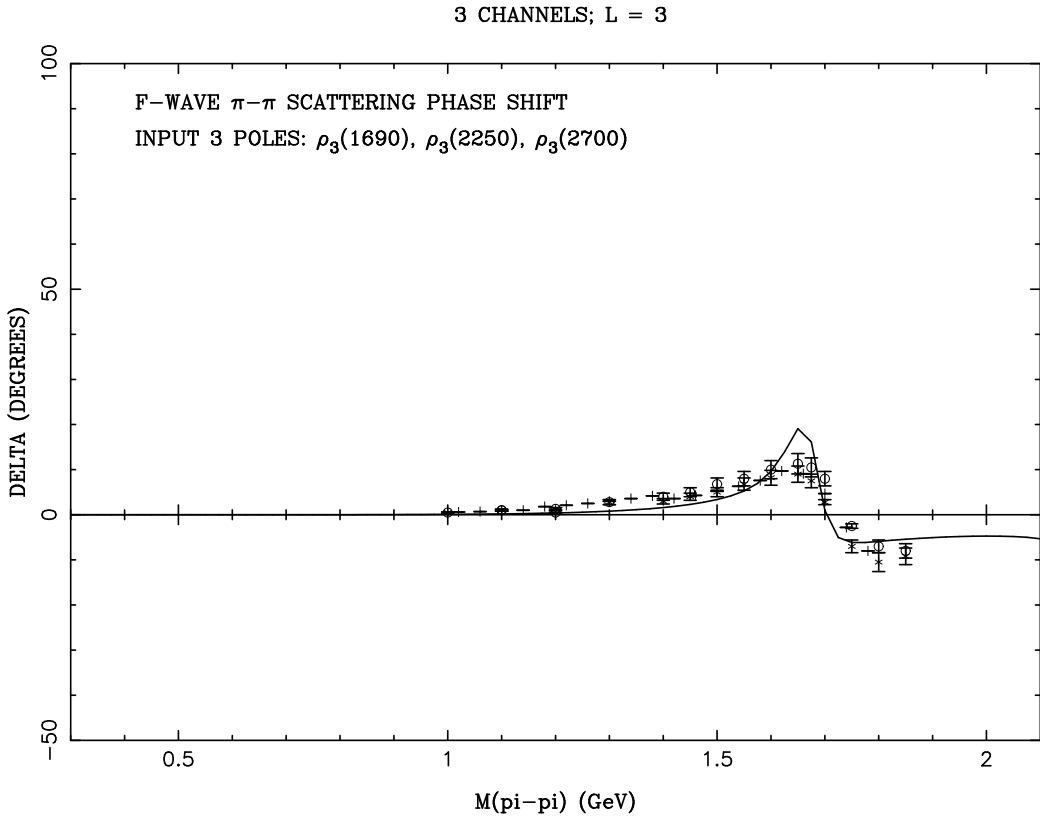

FIG. 9. F-wave $\pi\pi$ phase shifts from the three-channel model, if poles are present for $\rho_3(1690)$, $\rho_3(2250)$ and $\rho_3(2700)$. Solid curve is the prediction for the $l = 3$ parameter set from Table VI. Data are from Refs. [12,13].

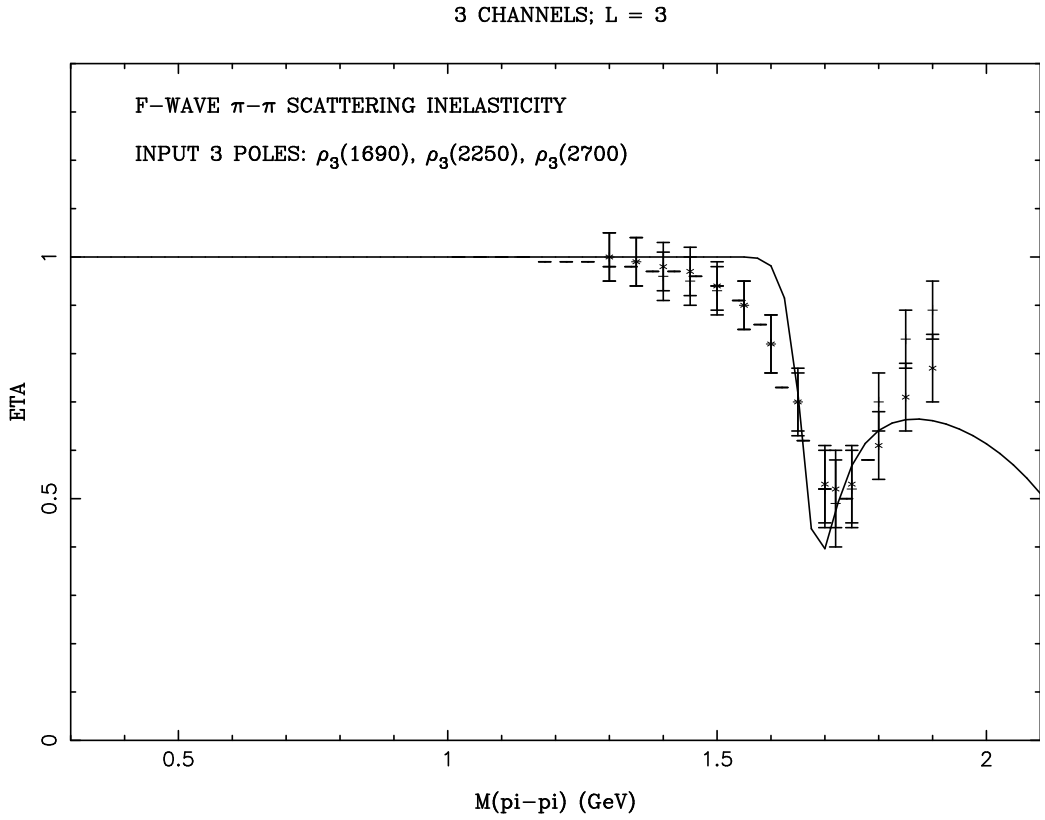

FIG. 10. F-wave $\pi\pi$ inelasticities from the three-channel model, if poles are present for $\rho_3(1690)$, $\rho_3(2250)$ and $\rho_3(2700)$. Solid curve is the prediction for the $l = 3$ parameter set from Table VI. Data are from Refs. [12,13].

TABLES

TABLE I. Relations of Λ_{ij} to λ_{ij} and R_i to X_i for angular momentum l.

l	Λ_i	Λ_{ij}^2	R_i
0	$\lambda_{ii}/(2\beta_i^3)$	$\lambda_{ij}^2/(4\beta_i^3\beta_j^3)$	$1/(2\beta_i^3 X_i)$
1	$\lambda_{ii}/(16\beta_i^5)$	$\lambda_{ij}^2/(256\beta_i^5\beta_j^5)$	$1/(16\beta_i^5 X_i)$
2	$\lambda_{ii}/(256\beta_i^7)$	$\lambda_{ij}^2/(256^2\beta_i^7\beta_j^7)$	$1/(256\beta_i^7 X_i)$
3	$\lambda_{ii}/(2048\beta_i^9)$	$\lambda_{ij}^2/(2048^2\beta_i^9\beta_j^9)$	$1/(2048\beta_i^9 X_i)$

TABLE II. Particle Data resonances considered in this work.

$J^\pi(I)$	$0^+(0)$	$1^-(1)$	$2^+(0)$	$3^-(1)$
—	$f_0(980)$	$\rho(770)$	$f_2(1270)$	$\rho_3(1690)$
—	$f_0(1370)$	$\rho(1450)$	$f_2(1525)$	$\rho_3(2250)$
—	$f_0(1500)$	$\rho(1700)$	$f_2(1710)$?	$\rho_3(2700)$
—	$f_0(1710)$?	$\rho(2150)$	$f_2(2010)$	—

TABLE III. Different model parameters for $l = 0$, i.e. $J^\pi(I) = 0^+(0)$ (β in GeV), Figs. 1 – 4.

β_0	β_1	β_2	β_3	Λ_0	Λ_1	Λ_2	Λ_3	Λ_{12}	Λ_{13}	Λ_{23}
2.80	0.85	0.40	1.75	-2.30	4.05	-0.158	-1.300	0.5523	0.0399	0.5425
3.60	1.35	0.50	0.25	-2.70	3.95	-0.678	-5.561	0.3059	0.3173	2.0061
3.80	1.25	0.20	1.00	-2.40	3.80	-0.946	-1.575	0.1689	0.3487	1.2793
2.80	0.85	0.30	3.25	-2.30	4.20	-0.124	-1.013	0.5646	0.3230	0.4532
4.00	1.25	0.30	0.50	-2.30	3.70	-0.914	-2.656	0.1333	0.5098	1.6397

TABLE IV. Different model parameters for $l = 2$, i.e. $J^\pi(I) = 2^+(0)$ (β in GeV), Figs. 5 – 6.

β_1	β_2	β_3	Λ_1	Λ_2	Λ_3	Λ_{12}	Λ_{13}	Λ_{23}
2.400	1.900	0.750	-0.210	-0.252	-0.050	0.0428	0.1222	0.0095
3.600	0.300	1.750	-0.300	1.596	-0.321	0.1059	0.0107	0.0977

TABLE V. Different model parameters for $l = 1$, i.e. $J^\pi(I) = 1^-(1)$ (β in GeV), Figs. 7 – 8.

β_1	β_2	β_3	Λ_1	Λ_2	Λ_3	Λ_{12}	Λ_{13}	Λ_{23}
3.200	15.500	3.250	-0.855	-0.991	-1.051	0.0035	0.0843	0.0074
2.600	0.500	0.750	-0.560	2.966	-1.457	0.9756	0.4386	0.2775

TABLE VI. Model parameters for $l = 3$, i.e. $J^{\pi}(I) = 3^{-}(1)$ (β in GeV), Figs. 9 – 10.

β_1	β_2	β_3	Λ_1	Λ_2	Λ_3	Λ_{12}	Λ_{13}	Λ_{23}
3.800	6.500	0.750	-0.170	-0.188	0.048	0.0013	0.0413	0.0146